Giant-Atom Quantum Batteries: Lossless Energy Transfer via Interference Engineering

Ke-Xiong Yan,[1,2] Yang Liu,[3] Yang Xiao,[1] Jun-Hao Lin,[1] Jie Song,[4] Ye-Hong Chen,[1,2,5,*] Franco Nori,[2,6] and Yan Xia[1,5,†]

[1]*Fujian Key Laboratory of Quantum Information and Quantum Optics, College of Physics and Information Engineering, Fuzhou University, Fuzhou 350108, China*
[2]*Quantum Information Physics Theory Research Team, Center for Quantum Computing, RIKEN, Wako-shi, Saitama 351-0198, Japan*
[3]*Center for Joint Quantum Studies and Department of Physics, School of Science, Tianjin University, Tianjin 300350, China*
[4]*Department of Physics, Harbin Institute of Technology, Harbin 150001, China*
[5]*Institute of Quantum Science and Technology, Yanbian University, Yanji 133002, China*
[6]*Department of Physics, University of Michigan, Ann Arbor, Michigan 48109-1040, USA*

(Received 22 August 2025; revised 10 March 2026; accepted 7 April 2026; published 6 May 2026)

Environmentally induced decoherence leads to irreversible energy loss during the active charging and discharging processes of quantum batteries (QBs). To address this issue, we propose a charging protocol utilizing the nonlocal coupling properties of giant atoms (GAs). In this Letter, both the QB and its charger are implemented as superconducting GAs with multiple nonlocal coupling points to a shared microwave waveguide. By engineering these atoms in a braided configuration, where their coupling paths are spatially interleaved, we realize lossless energy transfer dynamics. This is achieved by exploiting destructive interference to suppress waveguide-mediated dissipation while simultaneously preserving coherent interactions between the charger and the QB. The charging properties of separated and nested coupled configurations are also investigated. The results show that these two configurations underperform the braided configuration. Additionally, we propose a long-range chiral charging protocol that facilitates unidirectional energy transfer between the charger and the battery, with the capability to reverse the flow direction by modulating the applied magnetic flux. Our results provide guidelines for implementing a decoherence-resistant charging protocol and remote chiral QBs in circuits with GA engineering.

DOI: 10.1103/43n6-rnj3

Introduction—As an energy storage device governed by quantum mechanical principles, quantum batteries (QBs) have emerged as one of the most promising applications related to future quantum technologies [1–9]. Distinct from classical counterparts, QBs fundamentally exploit quantum resources—such as quantum coherence and multipartite entanglement—to enable superior energy storage and transmission characteristics [10–12]. Theoretical investigations demonstrate that these nonclassical correlations can enhance key performance metrics: (i) exponentially accelerated charging power through collective quantum effects [13–19], (ii) superextensive scaling of storage capacity with system size [20–24], and (iii) nonequilibrium work extraction surpassing classical counterparts [25–27].

While QBs exhibit superior theoretical performance, their practical implementation faces two major challenges rooted in the inherent vulnerability of quantum systems. The first is the aging problem of the QB, primarily attributed to intrinsic, uncontrollable decoherence during the quiescent storage phase [28,29]. This has been addressed largely through internal structural protection, such as symmetry-protected decoherence-free subspaces [30], destructive interference-enabled dark-state engineering [31], and periodic-driving-modulated Floquet-engineered interactions [32]. The second, and perhaps more immediate challenge, is the irreversible energy loss during the active charging and discharging processes. Unlike the aging problem in the storage phase, suppressing such dynamical dissipation typically necessitates complex extrinsic control, including real-time quantum feedback with error correction [33], sophisticated environment engineering [34–36], or frequent projective measurements [37]. However, the realization of a self-protected, high-efficiency charging protocol in the field of QBs remains an open question.

In this Letter, we propose a foundational principle for lossless quantum energy transfer by leveraging the spatial configuration engineering of giant atoms (GAs). Unlike conventional pointlike atoms, GAs couple to a bosonic field at multiple discrete points separated by wavelengths [38], a feature that offers unprecedented control over Lamb shifts, individual relaxation, and collective decay through interference effects [39–41]. While prior research has utilized these nonlocal properties to demonstrate chiral bound states and unidirectional state transfer [42,43], their

[*]Contact author: yehong.chen@fzu.edu.cn
[†]Contact author: xia-208@163.com

potential for optimizing quantum energy transfer, specifically for achieving high-efficiency charging without energy loss, remains unexplored. Here, we show that by modulating the GA-waveguide interface, one can achieve a flexible and decoherence-immune charging protocol, providing a robust framework for remote energy management in quantum circuits.

In our protocol, two GAs (each coupled to a waveguide at two spatially separated points) are configured as the charger and battery element, respectively. We investigate the charging property of three different coupling configurations: braided, separated, and nested couplings [39].

When the two GAs are in a braided configuration, by engineering the distance between connection points, we can observe persistent energy transfer between the charger and battery without direct coupling.

Simultaneously, dominant and unavoidable decoherence channels (i.e., irreversible energy leakage into the waveguide) are eliminated due to their mutual interference, thereby achieving perfect, lossless energy transfer between the charger and the QB.

For the separated and nested structures, we find that the GAs of both configurations underperform the braided configuration in terms of charging performance due to the presence of dissipation in the charging process.

Furthermore, we investigate the possibility of separated GAs enabling remote chiral charging, where the term "remote" specifically denotes an effective charging distance that significantly exceeds the typical length scale of dipole-dipole coupling. The chiral state transfer mechanism in GAs was initially introduced in Refs. [44–46] and then subsequently validated in the experiment [47]. By leveraging this unique characteristic of GAs, we can achieve directional energy flow between the charger and the battery and evaluate the resulting charging process.

Model—The charging protocol consists of two GAs acting as the charger and the QB, in which each GA interacts with a common 1D waveguide through two separated coupling points, as shown in Fig. 1. The locations of these coupling points are labeled by the coordinates x_{jn}, with $j = a, b$ marking the GAs and $n = 1, 2$ denoting the two coupling points of each atom. Under the rotating-wave approximation, the system Hamiltonian reads (hereafter we set $\hbar = 1$)

$$H = \omega_0 \sum_{j=a,b} \sigma_j^+ \sigma_j^- + \sum_{k=-\infty}^{+\infty} [\omega_k a_k^\dagger a_k + \sum_{j=a,b} \sum_{n=1,2} (g_{jn} \sigma_j^+ a_k + \text{H.c.})], \tag{1}$$

where $\sigma_j^- = |g_j\rangle\langle e_j|$ is the transition operator from the excited state $|e_j\rangle$ to the ground state $|g_j\rangle$ with frequency ω_0 of the charger when $j = a$ and of the QB when $j = b$ and a_k is the annihilation operator of the kth mode with frequency ω_k in the waveguide. The constant term g_{jn} is the coupling strength related to the coupling points x_{jn}.

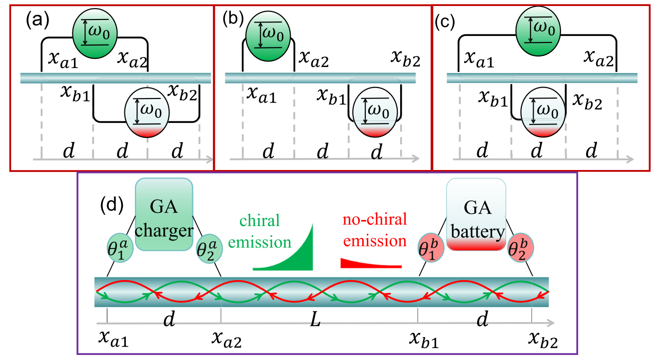

FIG. 1. Schematics of the (a) braided, (b) separated, and (c) nested configurations for double two-level GAs with energy separation ω_0 interacting with a common waveguide. (d) Schematic diagram of our remote chiral charging protocol. The phases $\theta_{1,2}^{a(b)}$ are modulated by the external magnetic flux.

Note that we apply the Wigner-Weisskopf approximation [48–50] in the weak-coupling regime, so the coupling strength can be treated as independent of k (k is the magnitude of the wave vector). For simplicity, we assume that the coupling strength at each connection point is g (i.e., $g_{jn} \equiv g$) and the distance between neighboring coupling points is d (see Fig. 1).

Charging performance—To investigate the charging performance of the two GAs, we treat the fields in the waveguide as the environment for the two GAs [51]. The evolution of the two atoms is governed by the quantum master equation. Assuming $\omega_{\pm k} \approx \omega_0 + (\pm k - k_0) v_g$, with k_0 (v_g) the wave number (group velocity) of the field at frequency ω_0 [52,53], the dynamics of the two GAs in these three different coupling configurations are governed by the unified master equation [51],

$$\dot{\rho}_I = -i[H_{\text{eff}}, \rho_I] + \sum_{j=a,b} \Gamma_j D[\sigma_j^-] + \Gamma_{\text{coll}} \{D[\sigma_a^-, \sigma_b^+] + \text{H.c.}\}, \tag{2}$$

where $D[A] = A\rho_I A^\dagger - 1/2(A^\dagger A \rho_I + \rho_I A^\dagger A)$, $D[A, B] = A\rho_I B^\dagger - 1/2(A^\dagger B \rho_I + \rho_I A^\dagger B)$, $\Gamma_{j=a,b} = \sum_{n,m=1,2} \gamma \cos(k_0|x_{jn} - x_{jm}|)$ and $\Gamma_{\text{coll}} = \sum_{n,m=1,2} \gamma \cos(k_0|x_{an} - x_{bm}|)$ are the individual and collective decay rates of the GAs. The parameter $\gamma = 4\pi g^2/v_g$ is the bare relaxation rate at each connection point.

The effective Hamiltonian H_{eff} of the two GAs in Eq. (2) takes the form

$$H_{\text{eff}} = \sum_{j=a,b} \delta\omega_j \sigma_j^+ \sigma_j^- + \sum_{i \neq j} g_{ab} \sigma_i^+ \sigma_j^-, \tag{3}$$

where $\delta\omega_j = \sum_{n,m=1,2} \gamma \sin(k_0|x_{jn} - x_{jm}|)/2$ is the Lamb shift of the jth GA and $g_{ab} = \sum_{n,m=1,2} \gamma \sin(k_0|x_{an} - x_{bm}|)/2$ is the exchange interaction strength. Note that

Eq. (2) is consistent with the quantum master equation derived by the SLH formalism in Ref. [39]. The Hamiltonian H_{eff} in Eq. (3) reveals that, although a direct charger-QB interaction is absent, an effective charger-QB coupling is induced by the mediation role of the electromagnetic fields in the waveguide.

QB performance indicators—In the process of charging, the charger is initialized to its excited state by a pump laser and then the QB is continuously energized from the charger [1,54]. The energy of the QB is

$$E(t) = \mathrm{Tr}[\rho_B(t) H_B], \tag{4}$$

where $H_B = \omega_0 \sigma_b^+ \sigma_b^-$ and $\rho_B(t) = \mathrm{Tr}_a[\rho_I]$. The maximal amount of work that can be extracted from a state $\rho_B(t)$ is provided by the ergotropy [1,25,27],

$$\mathcal{E}(t) = \mathrm{Tr}[\rho_B(t) H_B] - \mathrm{Tr}[\tilde{\rho}_B(t) H_B], \tag{5}$$

where $\tilde{\rho}_B(t) = \sum_m r_m(t) |s_m\rangle\langle s_m|$ is the passive state, $\{r_m(t)\}$ are the eigenvalues of $\rho_B(t)$ ordered in a descending sort, and $\{|s_m\rangle\}$ are the eigenstates of H_B with the corresponding eigenvalues s_m ordered in an ascending sort. The fluctuation between the initial and final time of the charging process is represented by the correlator [14,55]

$$\Sigma(t) = \left[\sqrt{\langle H_B^2(t)\rangle - \langle H_B(t)\rangle^2} - \sqrt{\langle H_B^2(0)\rangle - \langle H_B(0)\rangle^2}\right], \tag{6}$$

where $H_B(t)$ is the Heisenberg time evolution of the operator H_B. The average charging power of QB is given by [1]

$$\mathcal{P}(t) = \frac{\mathcal{E}(t)}{t}. \tag{7}$$

We investigate the charging property of the two GAs in the three different coupling configurations shown in Fig. 1. For each configuration, the initial state of the GA system is $|\psi(0)\rangle = |e_a\rangle|g_b\rangle$.

Charging characteristics of braided GAs—In the braided configuration, the two inner connection points are placed in between the two connection points of the other atoms, as shown in Fig. 1(a). We can obtain the Lamb shifts $\delta\omega_a = \delta\omega_b = \gamma \sin 2\theta$, the exchange coupling strength $g_{ab} = \gamma(3\sin\theta + \sin 3\theta)/2$, the individual decay rates $\Gamma_a = \Gamma_b = 2\gamma(1 + \cos 2\theta)$, and the collective decay rate $\Gamma_{\mathrm{coll}} = \gamma(3\cos\theta + \cos 3\theta)$ (see Supplemental Material [56] for details). The central parameter $\theta = k_0 d$ represents the propagation phase lag experienced by a photon traveling the distance d between the two coupling points. By substituting the expressions of g_{ab}, Γ_a, Γ_b, and Γ_{coll} into Eq. (2), the charging property of the two braided GAs can be analyzed.

In Fig. 2(a1), we plot the exchange interaction, the individual dissipation rate, and the collective dissipation rate of the two GAs as a function of the phase shift θ. It can be seen that both the individual and collective dissipation rates are zero when the phase shift $\theta = (n + 1/2)\pi$, with an integer n, while the exchange interaction is nonzero. Under this condition, the photon emission paths that lead to individual and collective dissipation of the GAs undergo complete destructive interference. Conversely, the photon emission paths that mediate the interaction between the GAs undergo partial destructive interference [56]. This suggests that lossless quantum energy transfer between the charger and the battery can be achieved when the distance between neighboring connection points is $d = (1 + 2n)\lambda_0/4$ in the braided configuration. The parameter $\lambda_0 = 2\pi v_g/\omega_0$ is the wavelength of the electromagnetic wave in the waveguide with frequency ω_0.

From Figs. 2(a2)–2(a4) we see that the ergotropy $\mathcal{E}$, the fluctuation Σ, and the average power $\mathcal{P}$ are modulated by the phase shift θ. Meanwhile, the dependence of $\mathcal{E}$, Σ, and $\mathcal{P}$ on θ is a π-period function. It can be found from Fig. 2(a2) that there are two ridges exhibiting a Rabi-like oscillating process when θ is near either $\pi/2$ or $3\pi/2$, implying a lossless energy transfer between the charger and the battery.

In particular, when $\theta = n\pi$, $\mathcal{E}$ approaches a steady value $0.25\omega_0$ in the long-time limit. This is because when $\theta \to n\pi$, we obtain $|\Gamma_{\mathrm{coll},a,b}| \to 0.4\omega_0$ and $g_{ab} \to 0$, which leads to the emergence of a steady state and a nonoscillatory charging process.

When $\theta = \pi/2$ or $\theta = 3\pi/2$, the energy fluctuation and charging power over time reflect the charging characteristics of the energy lossless charging process. During this charging process, the maximum average charging power is $0.072\omega_0$ and the maximum energy fluctuation is $0.5\omega_0$. This numerical result is consistent with the charging characteristic of the energy transfer process between two two-level atoms in a closed system [61]. When $\theta = n\pi$, the energy fluctuates as well as the average power does not oscillate over time. The maximum value of the average power and the maximum energy fluctuation during this charging process are $0.0407\omega_0$ and $0.4329\omega_0$, respectively.

Charging characteristics of separated GAs—We now turn to the case of two separated GAs, as shown in Fig. 1(b). In this configuration, we can obtain the Lamb shifts $\delta\omega_a = \delta\omega_b = \gamma \sin\theta$, the exchanging coupling strength $g_{ab} = \gamma(\sin\theta + 2\sin 2\theta + \sin 3\theta)/2$, the individual decay rates $\Gamma_a = \Gamma_b = 2\gamma(1 + \cos\theta)$, and the collective decay rate $\Gamma_{\mathrm{coll}} = \gamma(\cos\theta + 2\cos 2\theta + \cos 3\theta)$ (see Supplemental Material [56] for details). From Fig. 2(b1), it can be observed that when $\theta = \pi$, the interaction strength g_{ab} and the decay rates $\Gamma_{\mathrm{coll},a,b}$ become zero, indicating that the two separated GAs are decoupled from the waveguide. In the separated configuration, lossless charging of two GAs is not possible regardless of the value of θ. The maximum energy achievable

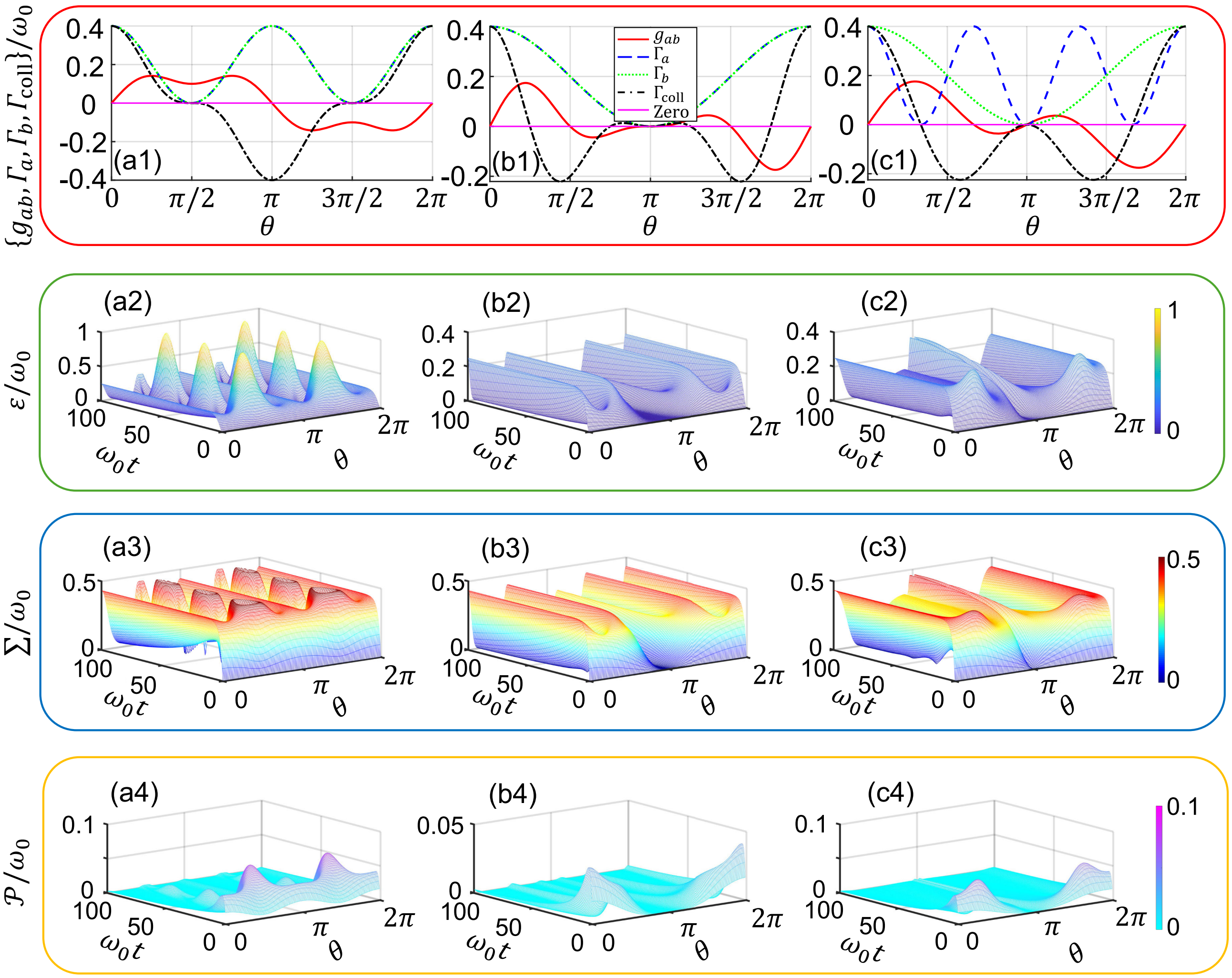

FIG. 2. Exchange interaction g_{ab} (red solid curve), individual decay rate Γ_a (blue dashed curve), individual decay rate Γ_b (green dotted curve), and collective decay rate $\Gamma_{\rm coll}$ (black dash-dot curve) as a function of θ for the braided (a1), separated (b1), and nested (c1) coupling configuration. (a2)–(c2) Ergotropy $\mathcal{E}$, (a3)–(c3) fluctuations Σ, and (a4)–(c4) average charging power $\mathcal{P}$, as functions of the scaled charging time $\omega_0 t$ and the accumulated phase θ. The parameter $\gamma = 0.1\omega_0$. For the braided configuration, at $\theta = \pi/2$ and $3\pi/2$, the Rabi-like oscillating ridges exhibited by $E(t)$ are a key feature, marking lossless coherent energy transfer. Under these phase conditions, $\Sigma(t)$ exhibits periodic oscillations, and $P(t)$ reaches its maximum value. When $\theta = \pi$, $\mathcal{E}(t)$ is in the steady-state region, exhibiting a nonoscillatory behavior. For the separated and nested configurations, $\mathcal{E}(t)$ cannot achieve a similar oscillatory process, regardless of the value of θ.

for the GA b as a battery is $0.250\omega_0$. The maximum energy fluctuation during charging and the maximum power are $0.443\omega_0$ and $0.040\omega_0$, respectively.

In Fig. 2(b2), there are four ridges with heights exceeding $0.2\omega_0$. These ridges do not oscillate with time, indicating that the system is in a steady state. When the phase shift $\theta = \pi$, the ergotropy $\mathcal{E}$, fluctuation Σ, and power $\mathcal{P}$ are all zero. This is caused by the inability of the charger and battery to produce indirect coupling through the waveguide. We can also find that the emergence of a nonoscillatory charging process when $\theta \to 0, 2\pi$, similar to the case of $\theta \to n\pi$ in the braided configuration. In Fig. 2(b3), the variation of energy fluctuations with the phase shift is similar to that of ergotropy. This is due to the nonoscillatory nature of the charging process, and a similar phenomenon is observed in the nested configuration. From Fig. 2(b4), we can see that the power reaches its maximum value only when $\theta = 0$ and $\theta = \pi$, which is a feature unique to the separated configuration.

Charging characteristics of nested GAs—Finally, we investigate the charging property for the nested coupling configuration, as depicted in Fig. 1(c). In this case, the relevant parameters in the quantum master equation (2) are given by $\delta\omega_a = \gamma\sin 3\theta$, $\delta\omega_b = \gamma\sin\theta$, $g_{ab} = \gamma(\sin\theta + \sin 2\theta)$, $\Gamma_a = 2\gamma(1 + \cos 3\theta)$, $\Gamma_b = 2\gamma(1 + \cos\theta)$, and $\Gamma_{\rm coll} = 2\gamma(\cos\theta + \cos 2\theta)$, respectively (see Supplemental Material [56] for details). From Fig. 2(c1), it can be found that the two GAs in the nested configuration are decoupled from the waveguide when $\theta = \pi$. When $\theta = 2n\pi$, the indirect interaction of the two GAs is zero, but the collective and individual dissipation rates into the waveguide reach a maximum, which can lead to the emergence of a nonoscillatory charging process.

From Figs. 2(c2)–2(c4), it can be found that the maximum values of the ergotropy, the energy fluctuation, and the average power are $0.329\omega_0$, $0.469\omega_0$, and $0.057\omega_0$, respectively. Both ergotropy $\mathcal{E}$ and fluctuations Σ converge rapidly to zero when $\theta \to \pi$. The physical mechanism behind this phenomenon is that the excitation paths of the two GAs interfere destructively, resulting in the absence of energy transfer channels between the two GAs and between the GAs and the waveguide. The same phenomenon occurs in both the nested and separated configurations, with the only difference being the rate at which the energy transfer channel disappears as the phase changes.

Remote chiral charging using GAs—In a long-distance chiral charging protocol [see Fig. 1(d)], GAs are suitable in a separated configuration. The distance between the charger and the battery is defined as $L = x_{b1} - x_{a2}$. To achieve unidirectional energy transfer, a phase difference must be introduced between the two coupling points of the GA. This can be accomplished by applying a magnetic flux $\Phi_{\rm ext}^{a(b)}$ that time-modulates each coupling point individually [44,62–65]. We assume that the phase difference between the two coupling points of the GA a and the GA b are $\theta^a = \theta_2^a - \theta_1^a$ and $\theta^b = \theta_2^b - \theta_1^b$, respectively. When the phase relation $\theta - \theta^{a(b)} = (2N+1)\pi$, the GAs decouple form the left-passing modes due to the destructive interference. We can obtain the Lamb shifts $\delta\omega_a = \delta\omega_b = -\gamma_{a(b)}(t)\sin 2\theta$ and the exchange coupling strength $g_{ab} = i\sqrt{\gamma_a(t)\gamma_b(t)}\sin^2\theta$. The jump operator for the master equation in Eq. (2) contains only the right-passing mode, i.e., $\dot{\rho}_I = -i[H_{\rm eff}, \rho_I] + D[L_R]$, where $H_{\rm eff} = \sum_{j=a,b} 1/2 (\omega_j + \delta\omega_j) + g_{ab}(\sigma_+^a\sigma_-^b - \text{H.c.})$, $L_R = i(\sqrt{\Gamma_a(t)/2}\sigma_-^a + \sqrt{\Gamma_b(t)/2}\sigma_-^b)$, and $\Gamma_{a(b)}(t) = 4(\sin\theta)^2\gamma_{a(b)}(t)$ (see Supplemental Material [56] for details).

By experimentally varying the magnetic flux at the coupling points [57,58], it becomes possible to control the coupling strength $g(t)$, thereby regulating the dissipation rates $\Gamma_{a(b)}(t)$ of each GA. When dissipation rates of the two GAs satisfy the function [59]

$$\Gamma_a(t) = \Gamma_b(\tau - t) = \begin{cases} \frac{\Gamma_{\max} e^{\Gamma_{\max}(t-\tau)}}{2 - e^{\Gamma_{\max}(t-\tau)}}, & t < \tau \\ \Gamma_{\max}, & t \geq \tau \end{cases}, \tag{8}$$

the evolution of the system satisfies the dark state condition [66], i.e., $L_R|\psi(t)\rangle = 0$, where $|\psi(t)\rangle$ is the state of the system at time t. That is, the system evolves through a state that is decoupled from the dissipative channel L_R, thus enabling lossless quantum energy transfer (see Supplemental Material [56] for details). The parameter τ represents the propagation time and is approximately given by $\tau \approx L/v_g$. Figures 3(b)–3(d) show the characteristics of the battery during the charging process. It can be observed that the flat ergotropy after a time of approximately 10 divided by $\Gamma_{\max}$ signifies successful, stable charging. When energy extraction from the battery is required, the phase conditions can be adjusted to reverse the direction of energy flow, enabling a unidirectional transfer from the battery back to the charger.

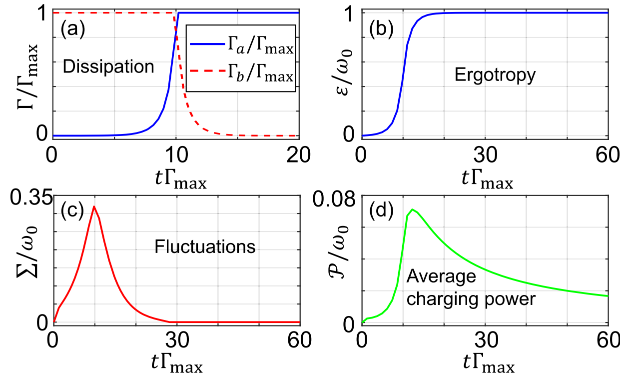

FIG. 3. (a) Dissipation of the two separated GAs with the propagation time $\tau = 10\Gamma_{\max}$. (b) Ergotropy $\mathcal{E}$, (c) fluctuations Σ, and (d) average charging power $\mathcal{P}$, as functions of the scaled charging time $\Gamma_{\max}t$. Here, $\Gamma_{\max}$ represents the maximum dissipation rate achievable by each GA, which is set to $0.1\omega_0$. All simulation results are obtained using the controlled dissipation profile defined by Eq. (8).

Conclusions—The QB protocol we proposed can be implemented in superconducting circuits [40,67]. Two frequency-tunable transmon qubits are coupled to a superconducting resonator for a dispersive readout [68]. Both qubits have two connections to a 50 Ω coplanar waveguide. The frequency of the qubit is set at $\omega_0/2\pi = 4$ GHz, dissipation rate of connection points are $\gamma/2\pi = 4$ MHz, and the phase accumulated by the propagation of the electromagnetic field in the waveguide between neighboring connection points is $\theta = \pi/2$. The maximum power $\mathcal{P}_{\max}/2\pi$ and maximum energy $\mathcal{E}_{\max}/2\pi$ of decoherence-immune charging between two braided GAs are 0.72 MHz and 4 GHz, respectively.

In summary, we have conducted a comprehensive analysis of GAs as models of QBs and assessed a remote chiral charging protocol. The results primarily highlight the substantial benefits of GAs in QB construction, including lossless energy transfer (high-efficiency charging) and chiral, remote charging. These capabilities are central to current QB research. Moreover, the proposed protocol offers flexible control over energy storage and extraction, all while maintaining immunity to external environmental noise (from waveguide). We hope that our proposed giant-atom quantum battery model can serve as a novel control paradigm to accelerate the development and implementation of advanced QB technologies.

Acknowledgments—We express sincere gratitude to Lei Du and Xin Wang for the insightful discussions and valuable suggestions. Y.-H. C. was supported by the National Natural Science Foundation of China under Grants No. 12304390 and No. 12574386, the National Postdoctoral Overseas Talent Recruitment Program of China, the Fujian 100 Talents Program, and the Fujian Minjiang Scholar Program. Y. X. was supported by the National Natural Science Foundation of China under Grant No. 62471143, the Key Program of National Natural Science Foundation of Fujian Province under Grant No. 2024J02008. F. N. was supported in part by the Japan Science and Technology Agency (JST) via the CREST Quantum Frontiers program Grant No. JPMJCR24I2, the Quantum Leap Flagship Program (Q-LEAP), the Moonshot R&D Grant No. JPMJMS2061, and the Office of Naval Research (ONR)Global (via Grant No. N62909-23-1-2074).

Data availability—The data that support the findings of this article are available from the authors upon reasonable request.

[1] F. Campaioli, S. Gherardini, J. Q. Quach, M. Polini, and G. M. Andolina, Colloquium: Quantum batteries, Rev. Mod. Phys. **96**, 031001 (2024).
[2] W.-L. Song, J.-L. Wang, B. Zhou, W.-L. Yang, and J.-H. An, Self-discharging mitigated quantum battery, Phys. Rev. Lett. **135**, 020405 (2025).
[3] F. Barra, Dissipative charging of a quantum battery, Phys. Rev. Lett. **122**, 210601 (2019).
[4] A. G. Catalano, S. M. Giampaolo, O. Morsch, V. Giovannetti, and F. Franchini, Frustrating quantum batteries, PRX Quantum **5**, 030319 (2024).
[5] B. Ahmadi, P. Mazurek, P. Horodecki, and S. Barzanjeh, Nonreciprocal quantum batteries, Phys. Rev. Lett. **132**, 210402 (2024).
[6] Z.-G. Lu, G. Tian, X.-Y. Lü, and C. Shang, Topological quantum batteries, Phys. Rev. Lett. **134**, 180401 (2025).
[7] F. Caravelli, G. Coulter-De Wit, L. P. García-Pintos, and A. Hamma, Random quantum batteries, Phys. Rev. Res. **2**, 023095 (2020).
[8] D.-L. Yang, F.-M. Yang, and F.-Q. Dou, Three-level Dicke quantum battery, Phys. Rev. B **109**, 235432 (2024).
[9] F.-M. Yang and F.-Q. Dou, Resonator-qutrit quantum battery, Phys. Rev. A **109**, 062432 (2024).
[10] K. V. Hovhannisyan, M. Perarnau-Llobet, M. Huber, and A. Acín, Entanglement generation is not necessary for optimal work extraction, Phys. Rev. Lett. **111**, 240401 (2013).
[11] F. C. Binder, S. Vinjanampathy, K. Modi, and J. Goold, Quantacell: Powerful charging of quantum batteries, New J. Phys. **17**, 075015 (2015).
[12] G. M. Andolina, M. Keck, A. Mari, M. Campisi, V. Giovannetti, and M. Polini, Extractable work, the role of correlations, and asymptotic freedom in quantum batteries, Phys. Rev. Lett. **122**, 047702 (2019).
[13] D. Ferraro, M. Campisi, G. M. Andolina, V. Pellegrini, and M. Polini, High-power collective charging of a solid-state quantum battery, Phys. Rev. Lett. **120**, 117702 (2018).
[14] A. Crescente, M. Carrega, M. Sassetti, and D. Ferraro, Ultrafast charging in a two-photon Dicke quantum battery, Phys. Rev. B **102**, 245407 (2020).
[15] J. Chen, L. Zhan, L. Shao, X. Zhang, Y. Zhang, and X. Wang, Charging quantum batteries with a general harmonic driving field, Ann. Phys. (Amsterdam) **532**, 1900487 (2020).
[16] L. Peng, W.-B. He, S. Chesi, H.-Q. Lin, and X.-W. Guan, Lower and upper bounds of quantum battery power in multiple central spin systems, Phys. Rev. A **103**, 052220 (2021).
[17] S. Julià-Farré, T. Salamon, A. Riera, M. N. Bera, and M. Lewenstein, Bounds on the capacity and power of quantum batteries, Phys. Rev. Res. **2**, 023113 (2020).
[18] J. Dias, H. Wang, K. Nemoto, N. Franco, and W. J. Munro, Efficient charging of multiple open quantum batteries through dissipation and pumping, Phys. Rev. A **113**, 012617 (2026).
[19] F. Campaioli, F. A. Pollock, F. C. Binder, L. Céleri, J. Goold, S. Vinjanampathy, and K. Modi, Enhancing the charging power of quantum batteries, Phys. Rev. Lett. **118**, 150601 (2017).
[20] Y. Wang, X. Huang, and T. Zhang, Distribution relationship of quantum battery capacity, Adv. Quantum Technol. **8**, 2400652 (2025).
[21] Y.-K. Wang, L.-Z. Ge, T. Zhang, S.-M. Fei, Y. Gao, and Z.-X. Wang, Dynamics of quantum battery capacity under Markovian channels, Quantum Inf. Process. **24**, 34 (2025).
[22] X. Yang, Y.-H. Yang, M. Alimuddin, R. Salvia, S.-M. Fei, L.-M. Zhao, S. Nimmrichter, and M.-X. Luo, Battery capacity of energy-storing quantum systems, Phys. Rev. Lett. **131**, 030402 (2023).
[23] F.-Q. Dou, H. Zhou, and J.-A. Sun, Cavity Heisenberg-spin-chain quantum battery, Phys. Rev. A **106**, 032212 (2022).
[24] F.-Q. Dou, Y.-Q. Lu, Y.-J. Wang, and J.-A. Sun, Extended Dicke quantum battery with interatomic interactions and driving field, Phys. Rev. B **105**, 115405 (2022).
[25] G. Francica, F. C. Binder, G. Guarnieri, M. T. Mitchison, J. Goold, and F. Plastina, Quantum coherence and ergotropy, Phys. Rev. Lett. **125**, 180603 (2020).
[26] H.-L. Shi, S. Ding, Q.-K. Wan, X.-H. Wang, and W.-L. Yang, Entanglement, coherence, and extractable work in quantum batteries, Phys. Rev. Lett. **129**, 130602 (2022).
[27] B. Çakmak, Ergotropy from coherences in an open quantum system, Phys. Rev. E **102**, 042111 (2020).
[28] F. Pirmoradian and K. Mølmer, Aging of a quantum battery, Phys. Rev. A **100**, 043833 (2019).
[29] F. Zhao, F.-Q. Dou, and Q. Zhao, Quantum battery of interacting spins with environmental noise, Phys. Rev. A **103**, 033715 (2021).
[30] J. Liu, D. Segal, and G. Hanna, Loss-free excitonic quantum battery, J. Phys. Chem. C **123**, 18303 (2019).
[31] J. Q. Quach and W. J. Munro, Using dark states to charge and stabilize open quantum batteries, Phys. Rev. Appl. **14**, 024092 (2020).

[32] S.-Y. Bai and J.-H. An, Floquet engineering to reactivate a dissipative quantum battery, Phys. Rev. A **102**, 060201(R) (2020).

[33] M. T. Mitchison, J. Goold, and J. Prior, Charging a quantum battery with linear feedback control, Quantum **5**, 500 (2021).

[34] K. Xu, H.-G. Li, Z.-G. Li, H.-J. Zhu, G.-F. Zhang, and W.-M. Liu, Charging performance of quantum batteries in a double-layer environment, Phys. Rev. A **106**, 012425 (2022).

[35] J. Carrasco, J. R. Maze, C. Hermann-Avigliano, and F. Barra, Collective enhancement in dissipative quantum batteries, Phys. Rev. E **105**, 064119 (2022).

[36] K. Xu, H.-J. Zhu, G.-F. Zhang, and W.-M. Liu, Enhancing the performance of an open quantum battery via environment engineering, Phys. Rev. E **104**, 064143 (2021).

[37] S. Gherardini, F. Campaioli, F. Caruso, and F. C. Binder, Stabilizing open quantum batteries by sequential measurements, Phys. Rev. Res. **2**, 013095 (2020).

[38] A. Frisk Kockum, P. Delsing, and G. Johansson, Designing frequency-dependent relaxation rates and Lamb shifts for a giant artificial atom, Phys. Rev. A **90**, 013837 (2014).

[39] A. F. Kockum, G. Johansson, and F. Nori, Decoherence-free interaction between giant atoms in waveguide quantum electrodynamics, Phys. Rev. Lett. **120**, 140404 (2018).

[40] A. F. Kockum and F. Nori, Quantum bits with Josephson junctions, in *Fundamentals and Frontiers of the Josephson Effect* (Springer International Publishing, New York, 2019) pp. 703–741.

[41] B. Kannan, M. J. Ruckriegel, D. L. Campbell, A. Frisk Kockum, J. Braumüller, D. K. Kim, M. Kjaergaard, P. Krantz, A. Melville, B. M. Niedzielski, A. Vepsäläinen, R. Winik, J. L. Yoder, F. Nori, T. P. Orlando, S. Gustavsson, and W. D. Oliver, Waveguide quantum electrodynamics with superconducting artificial giant atoms, Nature (London) **583**, 775 (2020).

[42] X. Wang, T. Liu, A. F. Kockum, H.-R. Li, and F. Nori, Tunable chiral bound states with giant atoms, Phys. Rev. Lett. **126**, 043602 (2021).

[43] Z.-Q. Wang, Y.-P. Wang, J. Yao, R.-C. Shen, W.-J. Wu, J. Qian, J. Li, S.-Y. Zhu, and J. Q. You, Giant spin ensembles in waveguide magnonics, Nat. Commun. **13**, 7580 (2022).

[44] X. Wang and H.-R. Li, Chiral quantum network with giant atoms, Quantum Sci. Technol. **7**, 035007 (2022).

[45] L. Du, Y. Zhang, J.-H. Wu, A. F. Kockum, and Y. Li, Giant atoms in a synthetic frequency dimension, Phys. Rev. Lett. **128**, 223602 (2022).

[46] Y.-T. Chen, L. Du, L. Guo, Z. Wang, Y. Zhang, Y. Li, and J.-H. Wu, Nonreciprocal and chiral single-photon scattering for giant atoms, Commun. Phys. **5**, 215 (2022).

[47] C. Joshi, F. Yang, and M. Mirhosseini, Resonance fluorescence of a chiral artificial atom, Phys. Rev. X **13**, 021039 (2023).

[48] D. F. Walls and G. J. Millburn, *Quantum Optics*, 2nd ed. (Springer, Berlin, 2008).

[49] G. S. Agarwal, *Quantum Optics* (Cambridge University Press, Cambridge, England, 2012).

[50] M. O. Scully and M. S. Zubairy, *Quantum Optics*, 1st ed. (Cambridge University Press, Cambridge, England, 1997).

[51] X.-L. Yin and J.-Q. Liao, Generation of two-giant-atom entanglement in waveguide-QED systems, Phys. Rev. A **108**, 023728 (2023).

[52] J.-T. Shen and S. Fan, Coherent single photon transport in a one-dimensional waveguide coupled with superconducting quantum bits, Phys. Rev. Lett. **95**, 213001 (2005).

[53] J.-T. Shen and S. Fan, Theory of single-photon transport in a single-mode waveguide. I. Coupling to a cavity containing a two-level atom, Phys. Rev. A **79**, 023837 (2009).

[54] W.-L. Song, H.-B. Liu, B. Zhou, W.-L. Yang, and J.-H. An, Remote charging and degradation suppression for the quantum battery, Phys. Rev. Lett. **132**, 090401 (2024).

[55] N. Friis and M. Huber, Precision and work fluctuations in Gaussian battery charging, Quantum **2**, 61 (2018).

[56] See Supplemental Material at http://link.aps.org/supplemental/10.1103/43n6-rnj3 for a detailed derivation of the SLH formalism, analysis of robustness to phase deviations, and details of the energy transfer process in chiral charging protocols, which includes Refs. [39,42,57–60].

[57] F. Wulschner *et al.*, Tunable coupling of transmission-line microwave resonators mediated by an RF SQUID, Eur. Phys. J. Quantum Technol. **3**, 10 (2016).

[58] M. R. Geller, E. Donate, Y. Chen, M. T. Fang, N. Leung, C. Neill, P. Roushan, and J. M. Martinis, Tunable coupler for superconducting X-mon qubits: Perturbative nonlinear model, Phys. Rev. A **92**, 012320 (2015).

[59] K. Stannigel, P. Rabl, A. S. Sørensen, M. D. Lukin, and P. Zoller, Optomechanical transducers for quantum-information processing, Phys. Rev. A **84**, 042341 (2011).

[60] W. Shao, C. Wu, and X.-L. Feng, Generalized James' effective Hamiltonian method, Phys. Rev. A **95**, 032124 (2017).

[61] G. M. Andolina, D. Farina, A. Mari, V. Pellegrini, V. Giovannetti, and M. Polini, Charger-mediated energy transfer in exactly solvable models for quantum batteries, Phys. Rev. B **98**, 205423 (2018).

[62] L. Zhou, Z. R. Gong, Y. X. Liu, C. P. Sun, and F. Nori, Controllable scattering of a single photon inside a one-dimensional resonator waveguide, Phys. Rev. Lett. **101**, 100501 (2008).

[63] J.-Q. Liao, Z. R. Gong, L. Zhou, Y. X. Liu, C. P. Sun, and F. Nori, Controlling the transport of single photons by tuning the frequency of either one or two cavities in an array of coupled cavities, Phys. Rev. A **81**, 042304 (2010).

[64] L. Zhou, S. Yang, Y. X. Liu, C. P. Sun, and F. Nori, Quantum Zeno switch for single-photon coherent transport, Phys. Rev. A **80**, 062109 (2009).

[65] L. Zhou, H. Dong, Y. X. Liu, C. P. Sun, and F. Nori, Quantum supercavity with atomic mirrors, Phys. Rev. A **78**, 063827 (2008).

[66] B. Vermersch, P.-O. Guimond, H. Pichler, and P. Zoller, Quantum state transfer via noisy photonic and phononic waveguides, Phys. Rev. Lett. **118**, 133601 (2017).

[67] X. Gu, A. F. Kockum, A. Miranowicz, Y.-X. Liu, and F. Nori, Microwave photonics with superconducting quantum circuits, Phys. Rep. **718–719**, 1 (2017).

[68] A. Blais, R.-S. Huang, A. Wallraff, S. M. Girvin, and R. J. Schoelkopf, Cavity quantum electrodynamics for superconducting electrical circuits: An architecture for quantum computation, Phys. Rev. A **69**, 062320 (2004).